SUPPLEMENTARY INFORMATION

Inhibition of fatty acid oxidation as a therapy for MYC-overexpressing triple-negative breast cancer

Roman Camarda, Alicia Y. Zhou, Rebecca A. Kohnz, Sanjeev Balakrishnan, Celine Mahieu, Brittany Anderton, Henok Eyob, Shingo Kajimura, Aaron Tward, Gregor Krings, Daniel K. Nomura, and Andrei Goga

Supplementary Table 1 Metabolomic changes in MTB-TOM tumors compared to non-tumor mammary glands. All differential metabolite abundance analyses were performed using the *limma* R package.

Supplementary Figure 1 Metabolic pathway alterations in MTB-TOM tumors compared to non-tumor mammary glands. Differential abundance of metabolites in five metabolic pathways commonly associated with tumorigenesis (amino acid, nucleotide, glycolysis, TCA cycle and pentose phosphate pathway) is shown. Detected metabolites were grouped by pathway (although many of these metabolites are intermediates in multiple pathways), and unbiased hierarchical clustering was used to display relative abundance of metabolites in MTB-TOM tumor versus non-tumor mammary gland. All differential metabolite abundance analyses were performed using the *limma* R package.

Supplementary Table 2 List of genes associated with fatty acid metabolism by the Gene Ontology Database and their expression in TN compared to RP tumors from TCGA RNA-Seq data (771 patients). All differential gene expression analyses were performed using the *limma* R package.

Supplementary Figure 2 Correlation analyses of TN and RP tumors to TCGA TN fatty acid metabolism centroid. A matrix of average fatty acid metabolism expression values was calculated for TCGA TN tumors. A sample-wise correlation analysis within each cohort against the TCGA TN centroid reveals the expression pattern to be significantly TN-specific (for *P*-values see **Supplementary Table 3**).

Supplementary Table 3 Correlation analyses of TN and RP tumors to TCGA TN fatty acid metabolism centroid. Similarities between this centroid and gene expression profiles of samples from the four independent clinical cohorts were quantified using Pearson correlation.

Supplementary Table 4 Univariate analysis indicating the effect of fatty acid metabolism gene expression on survival of all, TN and RP patients in a pooled neoadjuvant chemotherapy (taxane-anthracycline) treated cohort. Hazard ratio is

associated with a one standard deviation in gene expression. *P* values are based on the likelihood ratio test.

Supplementary Figure 3 Effect of etomoxir on TNBC cell proliferation and viability. Indicated cell types were treated with vehicle (dH_2O) or 200 μM etomoxir for 24, 48 or 72 h. Cell growth plots showing effect of etomoxir on proliferation. Viability assay showing effect of etomoxir on viability. A two-tailed unpaired *t*-test was used to compare etomoxir-treated (red) to untreated (blue) cells. Values shown are mean ± s.e.m. from three biological replicates. *$P \leq 0.05$

Supplementary Figure 4 Indicated cell types were treated with 30 pmol of CPT2 (M-008574-01) or non-targeting (D-001810-10-20) siRNA pool for 72 h, then examined by immunoblotting for indicated protein expression.

Supplementary Figure 5 Effects of matrix detachment on TN MYC^{high}, TN MYC^{low} and RP cells. Brightfield images of indicated cell lines 4 d after being seeded in ultra-low adhesion plates. After 4 d, indicated cell types were treated with 200 μM etomoxir or vehicle control for 48 h and ATP was measured. A two-tailed unpaired *t*-test was used to compare response of etomoxir-treated to untreated cells. Values shown are mean ± s.e.m. from five technical replicates. Number of biological replicates is indicated. ****$P < 0.0001$

Supplementary Figure 6 Effects of glucose starvation and/or etomoxir on TN MYC^{high}, TN MYC^{low} and RP cells. Indicated cell types were treated with glucose-depleted medium and/or 200 μM etomoxir or vehicle control for 24 h and ATP was measured. A two-tailed unpaired *t*-test was used to compare response of treated to untreated cells. Values shown are mean ± s.e.m. from triplicate samples. Number of biological replicates is indicated. ***$P < 0.001$, ****$P < 0.0001$

Supplementary Figure 7 Indicated cell types were examined by immunoblotting for indicated protein expression.

Supplementary Figure 8 Indicated cell types were treated with 30 pmol of MYC (L-003282-02-0005) or non-targeting (D-001810-10-20) siRNA pool for 72 h, then examined by immunoblotting for indicated protein expression.

Supplementary Table 5 Metabolomic changes in HCI-002 untreated tumors compared to 60 mg/kg etomoxir-treated tumors. All differential metabolite abundance analyses were performed using the *limma* R package.

Supplementary Figure 9 Effects of etomoxir on metabolite levels in MTB-TOM tumors. MTB-TOM allografts were treated with 20 mg/kg daily via IP injection for 14 d. Fold change in metabolite levels in etomoxir-treated xenografts versus vehicle-treated tumors are shown. A two-tailed unpaired *t*-test was used to compare metabolite levels in etomoxir-treated to untreated tumors. Values are shown as min-to-max box plots from

six mice in the control group and seven mice in the etomoxir-treated group. ^$P \leq 0.10$, *$P \leq 0.05$, **$P < 0.01$

Supplementary Table 6 Metabolomic changes in MTB-TOM untreated tumors compared to 20 mg/kg etomoxir-treated tumors. All differential metabolite abundance analyses were performed using the *limma* R package.

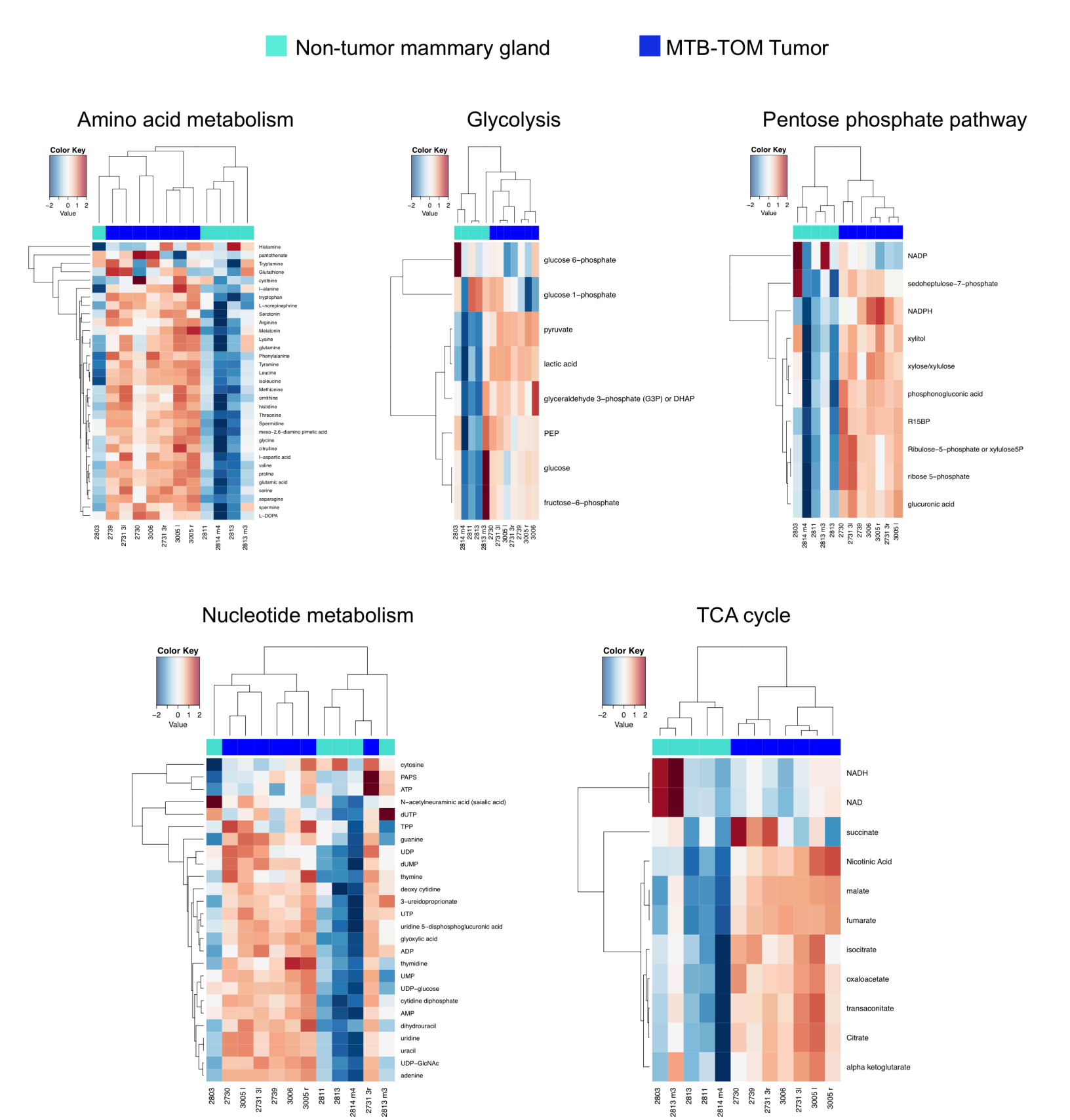

Supplementary Figure 1

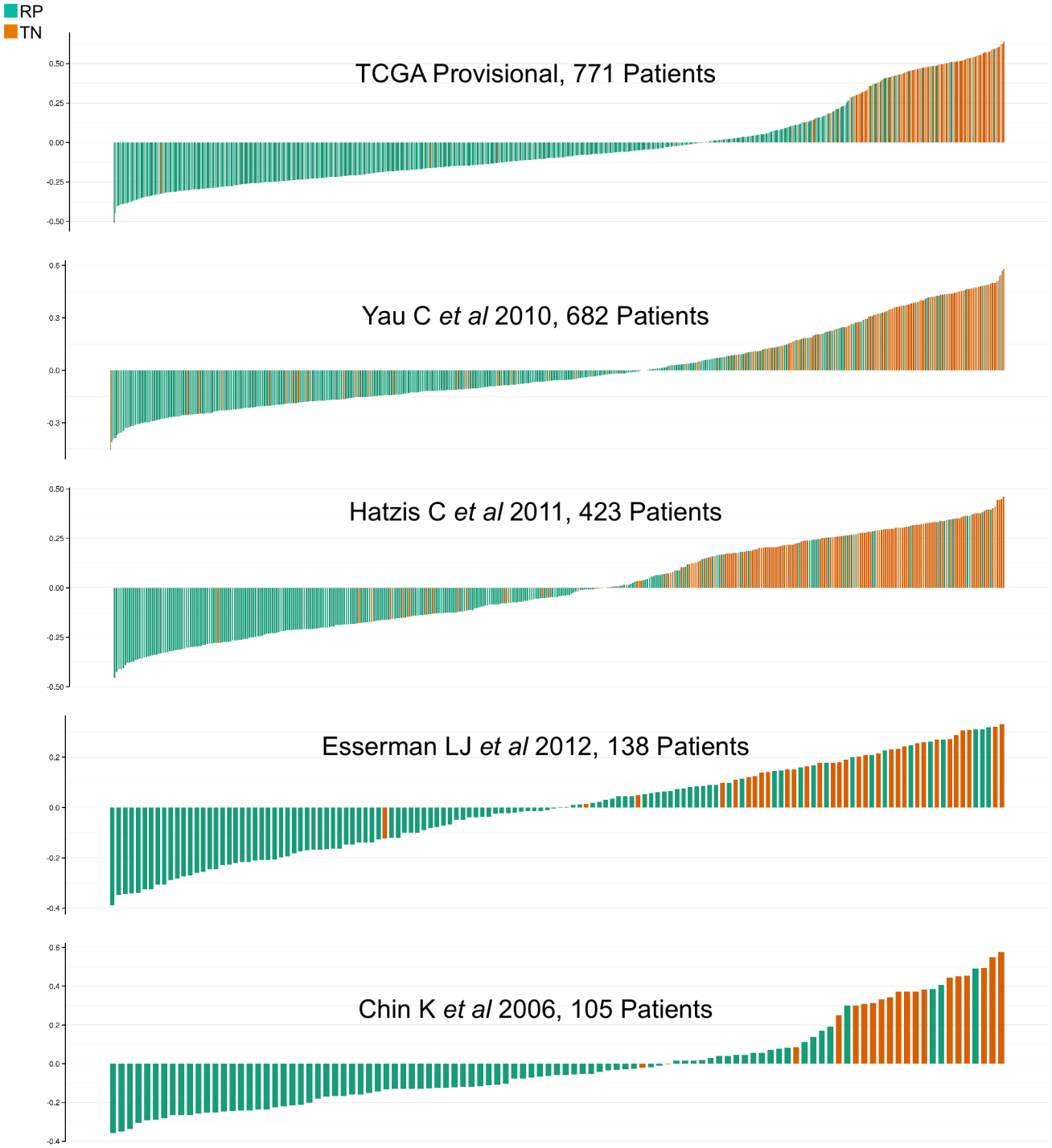

Supplementary Figure 2

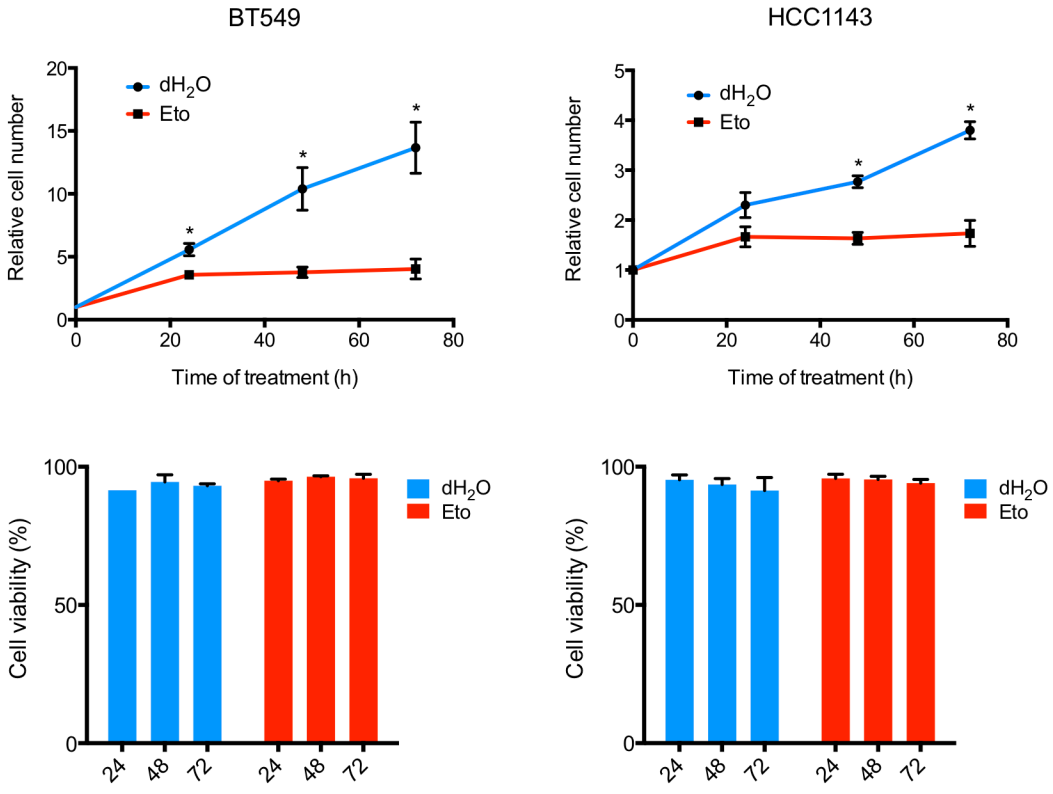

Supplementary Figure 3

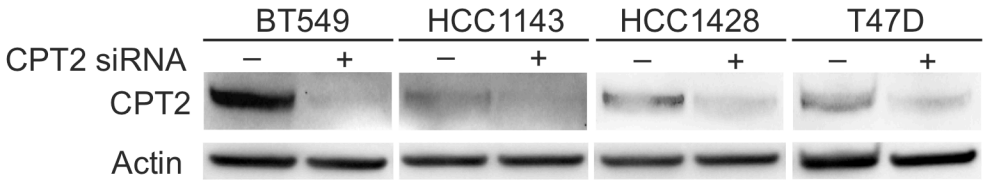

Supplementary Figure 4

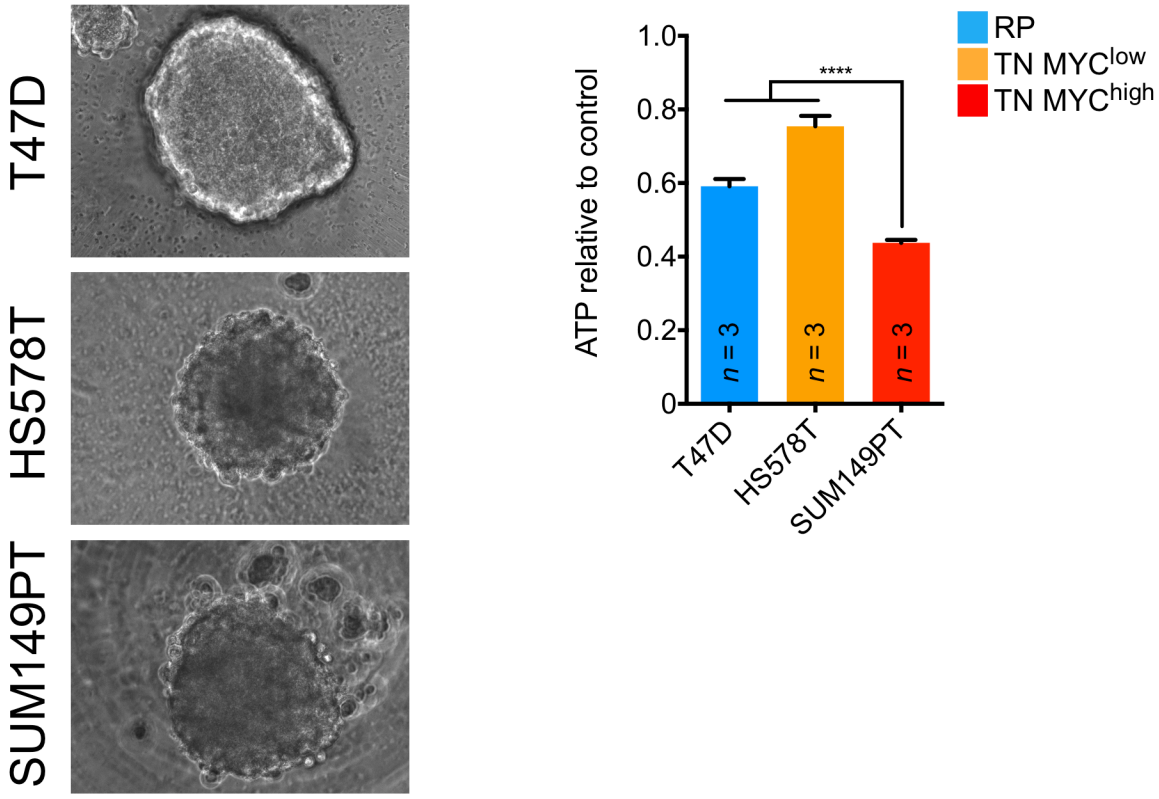

Supplementary Figure 5

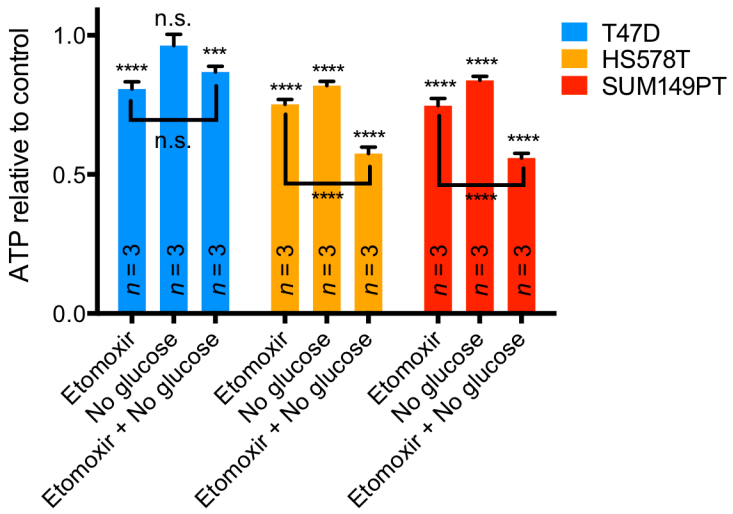

Supplementary Figure 6

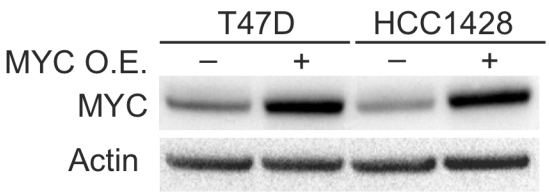

Supplementary Figure 7

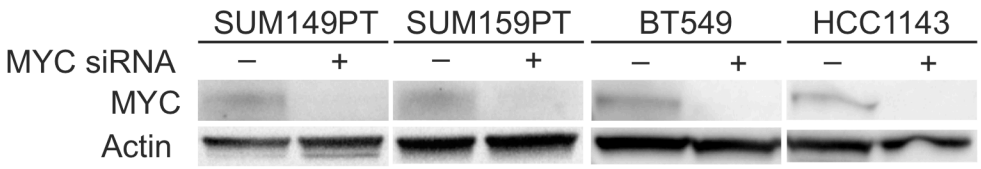

Supplementary Figure 8

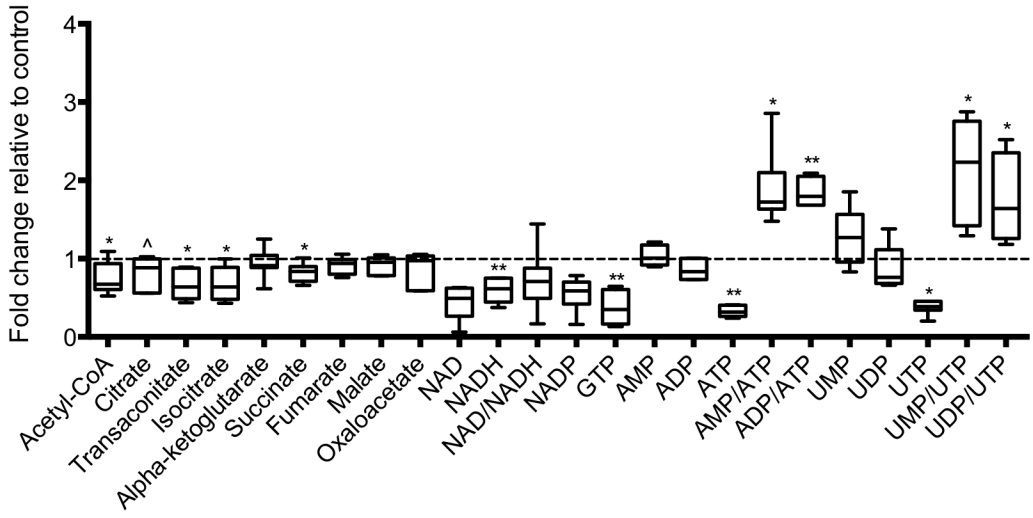

Supplementary Figure 9